Chapter 48
A Modal Test Method Based on Vibro-acoustical Reciprocity

W.D. Zhu, J.M. Liu, Y.F. Xu, and H.Q. Ying

Abstract A modal test method that uses sound pressure transducers at fixed locations and an impact hammer roving over a test structure is developed in this work. Since sound pressure transducers are used, the current method deals with a coupled structural-acoustic system. Based on the vibro-acoustic reciprocity, the method is equivalent to the one, where acoustic excitations at fixed locations are given and the resulting acceleration of the test structure is measured. The current method can eliminate mass loading due to the use of accelerometers, which can destroy the existence of repeated or close natural frequencies of a symmetric structure, avoid the effects of a nodal line of a mode and an inactive area of a local mode, and measure all the out-of-plane modes within a frequency range of interest, including global and local ones. The coupling between the structure and the acoustic field in a structural-acoustic system introduces asymmetry in the model formulation. An equivalent state space formulation is used for a structurally damped structural-acoustic system and the associated eigenvalue problem is derived. The biorthonormality relations between the left and right eigenvectors and the relations between the structural and acoustic components in the left and right eigenvectors are proved. The frequency response functions associated with the current method are derived and their physical meanings are explained. The guidelines for using the current method, including the types of structures that are suitable for the method, the positions of the sound pressure transducers, and the orientation of the test structure relative to the transducers, are provided. Modal tests were carried out on an automotive disk brake using the traditional and current methods, where multiple accelerometers and microphones were used to measure its dynamic responses induced by impacts, respectively. The measured natural frequencies and mode shapes by the two methods are almost the same. The differences between the measured natural frequencies using the current method and those from the finite element model of the disk brake are less than 3% for the first 18 elastic modes, and the modal assurance criterion values of the associated mode shapes are all above 90%.

Keywords Vibro-acoustic modal test • Vibro-acoustic reciprocity • Experimental modal analysis • Symmetric structure • Model validation

W.D. Zhu (✉)
Professor, Department of Mechanical Engineering, University of Maryland, Baltimore County, Baltimore, MD 21250, USA
e-mail: wzhu@umbc.edu

J.M. Liu
Research Scientist, China Orient Institute of Noise and Vibration, Beijing 100085, China
e-mail: jhgo1965@yahoo.com.cn

Y.F. Xu
Graduate Assistant, Department of Mechanical Engineering, University of Maryland, Baltimore County, Baltimore, MD 21250, USA
e-mail: yxu2@umbc.edu

H.Q. Ying
Professor, China Orient Institute of Noise and Vibration, Beijing 100085, China
e-mail: dasp@coinv.com.cn

R. Allemang et al. (eds.), *Topics in Modal Analysis, Volume 7: Proceedings of the 31st IMAC, A Conference on Structural Dynamics, 2013*, Conference Proceedings of the Society for Experimental Mechanics Series 45,
DOI 10.1007/978-1-4614-6585-0_48,

48.1 Introduction

Experimental modal analysis (EMA) is one of the standard experimental approaches to validate the finite element (FE) model of a structure, where the input to the test structure is in the form of a force and the output from the structure a displacement, velocity, or acceleration response [1, 2]. When the roving hammer technique is used in EMA, a measurement point is fixed on the test structure and an impact hammer roves over the structure. The location of the measurement point is crucial since some mode may not be captured in the test if the measurement point lies on a nodal line of a mode [3] or in an inactive area of a local mode. In order to mitigate the problem, EMA can be conducted using multiple measurement points at different locations. However, it can be difficult to find the proper locations for the measurement points at which all the modes of interest can be captured unless an accurate FE model of the structure is available, providing accurate mode shape information. On the other hand, mass loading due to the use of multiple sensors on the test structure can affect the accuracy of measurement [4], especially for a symmetric structure, whose repeated or close natural frequencies can be destroyed. A laser vibrometer can be used to avoid mass loading in EMA, but it may not be available in many laboratories. Another critical aspect of EMA is the excitation method. A shaker can be connected to the test structure to generate a prescribed excitation force, but the response measurements, especially in the neighborhoods of resonant frequencies, can have low signal-to-noise ratios due to impedance mismatch between the shaker and the test structure [5]. An impact hammer can be used in EMA, but the sensors attached on the structure far away from the excitation point may not capture much vibration. While acoustic excitation can excite the surface of the test structure, it is difficult to measure the acoustic excitation on the surface of the structure. An acoustic modal analysis method was proposed in [6] to measure the modal characteristics of a structure by using an impact hammer and microphones, and the time delay due to the use of microphones was corrected [7]. However, the method does not consider the effects of the structural-acoustic coupling. When acoustic excitation or measurement is involved in a modal test, coupling exists in the corresponding structural-acoustic system, and asymmetry is introduced in the model formulation [8, 9]. As a result, left and right eigenvectors can be defined for the associated eigenvalue problem, and the relations between the structural and acoustic components in the left and right eigenvectors of an undamped coupled system were provided in [10]. The formulation of a damped structural-acoustic system was given for a closed cavity in [11].

In this work, a vibro-acoustic modal test (VMT) method is developed, where an impact hammer roves over the test structure and sound pressure transducers at fixed locations are used to measure its dynamic responses. The formulation of a structurally damped structural-acoustic system in an open environment and the associated eigenvalue problem are provided. The biorthonormality relations between the left and right eigenvectors and the relations between the structural and acoustic components of the left and right eigenvectors are proved. The frequency response functions (FRFs) used in the VMT method are derived, which contain the modal characteristics of the coupled system, and the assumptions used in the acoustic modal analysis in [6, 7] are validated. It is assumed in the VMT method that the natural frequencies and the structural components of the right eigenvectors of the coupled system can be used to approximate the natural frequencies and mode shapes of the structure. Based on the vibro-acoustic reciprocity, the VMT method is equivalent to the one, where acoustic excitation sources are used to excite the test structure and the resulting acceleration is measured, and the guidelines for using the VMT method, including the types of structures that are suitable for the method, the positions of the sound pressure transducers, and the orientation of the test structure relative to the transducers, are provided. The VMT method and EMA were carried out on an automotive disk brake and the experimental results were compared. It is experimentally shown that the VMT method can capture all the out-of-plane modes, including global and local ones, and EMA can miss certain modes. The differences between the measured natural frequencies of the first 18 elastic modes by the VMT method and EMA are less than 1% and the modal assurance criterion (MAC) values [1] of the associated modes are all above 90%. The errors between the measured natural frequencies by the VMT method and the calculated ones from the FE model are less than 3% for the first 18 elastic modes, and the associated MAC values are all above 90%.

48.2 Structural-Acoustic System Formulation

48.2.1 Eigenvalue Problem

The FE formulation of an undamped, coupled structural-acoustic system has been given in [8, 9] using a displacement-pressure model for a closed cavity. A similar FE formulation has been given in [12] for a coupled fluid-structural system, based on which the FE formulation of a coupled structural-acoustic system in an open environment can be obtained. To apply this formulation, it is assumed that the structure is totally submerged in air and the effects of the boundary of air can

be neglected, which yields the following governing equation:

$$\begin{bmatrix} M_s & 0 \\ M_c & M_a \end{bmatrix} \begin{Bmatrix} \ddot{u}_s \\ \ddot{p}_a \end{Bmatrix} + \begin{bmatrix} K_s & K_c \\ 0 & K_a \end{bmatrix} \begin{Bmatrix} u_s \\ p_a \end{Bmatrix} = \begin{Bmatrix} f_s \\ f_a \end{Bmatrix} \tag{48.1}$$

where u_s is the n-dimensional displacement vector of the structure and p_a is the m-dimensional sound pressure vector of the acoustic field; f_s is the n-dimensional structural force vector and f_a is the m-dimensional sound source in the acoustic field; M_s and K_s are the $n \times n$ structural mass and stiffness matrices, respectively; M_a and K_a are the $m \times m$ acoustic mass and stiffness matrices, respectively; and M_c and K_c are the coupling matrices of the system of dimensions $m \times n$ and $n \times m$, respectively. Note that M_s, M_a, K_s, and K_a are symmetric. In Eq. (48.1), the upper and lower equations represent the structural and acoustic parts of the system, respectively. The relationship between the two coupling matrices can be expressed by [12]

$$M_c = -K_C^T \tag{48.2}$$

A similar relation between the two coupling matrices has been derived for a closed cavity [8–10]. Assume that viscous damping effects exist in the structural part in Eq. (48.1) and those in the acoustic part can be neglected; no coupling exists between the structural and acoustic damping [13]. Adding structural damping to Eq. (48.1) yields

$$\begin{bmatrix} M_s & 0 \\ M_c & M_a \end{bmatrix} \begin{Bmatrix} \ddot{u}_s \\ \ddot{p}_a \end{Bmatrix} + \begin{bmatrix} C_s & 0 \\ 0 & 0 \end{bmatrix} \begin{Bmatrix} \dot{u}_s \\ \dot{p}_a \end{Bmatrix} + \begin{bmatrix} K_s & K_c \\ 0 & K_a \end{bmatrix} \begin{Bmatrix} u_s \\ p_a \end{Bmatrix} = \begin{Bmatrix} f_s \\ f_a \end{Bmatrix} \tag{48.3}$$

where C_s is the symmetric structural damping matrix of dimensions $n \times n$. In order to determine the natural frequencies and mode shapes of the structural-acoustic system, it is assumed that the system has no excitation, which yields the following equation:

$$\begin{bmatrix} M_s & 0 \\ M_c & M_a \end{bmatrix} \begin{Bmatrix} \ddot{u}_s \\ \ddot{p}_a \end{Bmatrix} + \begin{bmatrix} C_s & 0 \\ 0 & 0 \end{bmatrix} \begin{Bmatrix} \dot{u}_s \\ \dot{p}_a \end{Bmatrix} + \begin{bmatrix} K_s & K_c \\ 0 & K_a \end{bmatrix} \begin{Bmatrix} u_s \\ p_a \end{Bmatrix} = \begin{Bmatrix} 0 \\ 0 \end{Bmatrix} \tag{48.4}$$

Due to the coupling between the structure and the acoustic field, it is difficult to directly solve Eq. (48.4). Let

$$\tilde{M} = \begin{bmatrix} M_s & 0 \\ M_c & M_a \end{bmatrix}, \tilde{C} = \begin{bmatrix} C_s & 0 \\ 0 & 0 \end{bmatrix}, \tilde{K} = \begin{bmatrix} K_s & K_c \\ 0 & K_a \end{bmatrix}, \ y = \begin{Bmatrix} u_s \\ p_a \end{Bmatrix} \tag{48.5}$$

Equation (48.4) can be written in an equivalent state space form:

$$\begin{bmatrix} -\tilde{K} & 0 \\ 0 & \tilde{M} \end{bmatrix} \begin{Bmatrix} \dot{y} \\ \ddot{y} \end{Bmatrix} + \begin{bmatrix} 0 & \tilde{K} \\ \tilde{K} & \tilde{C} \end{bmatrix} \begin{Bmatrix} y \\ \dot{y} \end{Bmatrix} = \begin{Bmatrix} 0 \\ 0 \end{Bmatrix} \tag{48.6}$$

The solution to Eq. (48.6) is assumed in the form

$$\begin{Bmatrix} y \\ \dot{y} \end{Bmatrix} = \begin{Bmatrix} ve^{\lambda t} \\ \lambda v e^{\lambda t} \end{Bmatrix} \tag{48.7}$$

where λ is an undetermined constant and v is an $(n + m)$-dimensional vector. Let

$$\eta = \begin{Bmatrix} v \\ \lambda v \end{Bmatrix} \tag{48.8}$$

and the following expressions can be obtained:

$$\begin{Bmatrix} y \\ \dot{y} \end{Bmatrix} = \eta e^{\lambda t}, \ \begin{Bmatrix} \dot{y} \\ \ddot{y} \end{Bmatrix} = \lambda \eta e^{\lambda t} \tag{48.9}$$

Substituting Eq. (48.9) into Eq. (48.6) and canceling $e^{\lambda t}$ yield

$$\lambda \begin{bmatrix} -\tilde{K} & 0 \\ 0 & \tilde{M} \end{bmatrix} \eta + \begin{bmatrix} 0 & \tilde{K} \\ \tilde{K} & C \end{bmatrix} \eta = \begin{Bmatrix} 0 \\ 0 \end{Bmatrix} \tag{48.10}$$

Let

$$S = \begin{bmatrix} -\tilde{K} & 0 \\ 0 & \tilde{M} \end{bmatrix}, \; R = \begin{bmatrix} 0 & \tilde{K} \\ \tilde{K} & C \end{bmatrix} \tag{48.11}$$

and Eq. (48.10) can be written as a generalized eigenvalue problem associated with the structural-acoustic system:

$$(\lambda S + R)\,\eta = 0 \tag{48.12}$$

Due to asymmetry of the matrices S and R, there exist right and left eigenvectors of the eigenvalue problem in Eq. (48.12). Let η_i^r be the right eigenvector corresponding to the eigenvalue λ_i of the eigenvalue problem in Eq. (48.12), which satisfies

$$(\lambda_i S + R)\,\eta_i^r = 0 \tag{48.13}$$

The left eigenvector η_j^l satisfies

$$\eta_j^{lT}\left(\lambda_j S + R\right) = 0 \tag{48.14}$$

where the superscript T denotes the transpose of a matrix, or

$$\left(\lambda_j S^T + R^T\right)\eta_j^l = 0 \tag{48.15}$$

It is assumed that all the eigenvalues of the eigenvalue problem in Eq. (48.12) are distinct. Note that while the eigenvalues in Eqs. (48.13) and (48.14) are the same, the corresponding left and right eigenvectors are not the same [14]. Pre-multiplying Eq. (48.13) by η_j^{lT} yields

$$\eta_j^{lT}\,(\lambda_i S + R)\,\eta_i^r = 0 \tag{48.16}$$

Post-multiplying Eq. (48.14) by η_i^r yields

$$\eta_j^{lT}\left(\lambda_j S + R\right)\eta_i^r = 0 \tag{48.17}$$

Subtracting Eq. (48.17) from Eq. (48.16) yields

$$\left(\lambda_i - \lambda_j\right)\eta_j^{lT} S \eta_i^r = 0 \tag{48.18}$$

If $i \neq j$, since all the eigenvalues are distinct, by Eq. (48.18), one has

$$\eta_j^{lT} S \eta_i^r = 0 \tag{48.19}$$

Substituting Eq. (48.19) into Eq. (48.16) yields

$$\eta_j^{lT} R \eta_i^r = 0 \tag{48.20}$$

When $i = j$, the right and left eigenvectors can be normalized as follows:

$$\eta_i^{lT} S \eta_i^r = 1 \tag{48.21}$$

Using Eq. (48.21) in Eq. (48.16) yields

$$\eta_i^{lT} R \eta_i^r = -\lambda_i \tag{48.22}$$

Equations (48.19)–(48.22) are the biorthonormality relations between the left and right eigenvectors of the system.

Assuming that the structural and acoustic components in the left eigenvector η_i^l, which are ϕ_{si}^l and ϕ_{ai}^l, respectively, can be related to those in the right eigenvector η_i^r, which are ϕ_{si}^r and ϕ_{ai}^r, respectively:

$$\phi_{si}^l = a\phi_{si}^r, \; \phi_{ai}^l = b\phi_{ai}^r \tag{48.23}$$

then the left eigenvector η_i^l can be expressed by

$$\eta_i^l = \begin{Bmatrix} \phi_{si}^l \\ \phi_{ai}^l \\ \lambda_i \phi_{si}^l \\ \lambda_i \phi_{ai}^l \end{Bmatrix} = \begin{Bmatrix} a\phi_{si}^r \\ b\phi_{ai}^r \\ \lambda_i a\phi_{si}^r \\ \lambda_i b\phi_{ai}^r \end{Bmatrix} \tag{48.24}$$

Substituting Eq. (48.24) into Eq. (48.14) yields

$$\begin{cases} -a\phi_{si}^{rT}\lambda_i K_s + a\phi_{si}^{rT}\lambda_i K_s = 0 \\ -a\phi_{si}^{rT}\lambda_i K_c - b\phi_{ai}^{rT}\lambda_i K_s + a\phi_{si}^{rT}\lambda_i K_c + b\phi_{ai}^{rT}\lambda_i K_s = 0 \\ a\phi_{si}^{rT} K_s + a\phi_{si}^{rT}\lambda_i\left(\lambda_i M_s + C_s\right) + b\phi_{ai}^{rT}\lambda_i^2 M_c = 0 \\ a\phi_{si}^{rT} K_c + b\phi_{ai}^{rT} K_a + b\phi_{ai}^{rT}\lambda_i^2 M_a = 0 \end{cases} \tag{48.25}$$

Since the first two equations in Eq. (48.25) are identically satisfied, Eq. (48.25) becomes

$$\begin{cases} a\phi_{si}^{rT} K_s + a\phi_{si}^{rT}\lambda_i\left(\lambda_i M_s + C_s\right) + b\phi_{ai}^{rT}\lambda_i^2 M_c = 0 \\ a\phi_{si}^{rT} K_c + b\phi_{ai}^{rT} K_a + b\phi_{ai}^{rT}\lambda_i^2 M_a = 0 \end{cases} \tag{48.26}$$

Due to symmetry of K_s, K_a, M_s, and M_a, taking the transpose of Eq. (48.26) and using Eq. (48.2) in the resulting expressions yield

$$\begin{cases} aK_s\phi_{si}^{r} + a\lambda_i\left(\lambda_i M_s + C_s\right)\phi_{si}^{r} - b\lambda_i^2 K_c\phi_{ai}^{r} = 0 \\ -aM_c\phi_{si}^{r} + bK_a\phi_{ai}^{r} + b\lambda_i^2 M_a\phi_{ai}^{r} = 0 \end{cases} \tag{48.27}$$

Expanding Eq. (48.13) using Eqs. (48.8) and (48.11) yields

$$\begin{cases} -\lambda_i K_s\phi_{si}^{r} - \lambda_i K_c\phi_{ai}^{r} + \lambda_i K_s\phi_{si}^{r} + \lambda_i K_c\phi_{ai}^{r} = 0 \\ -\lambda_i K_a\phi_{si}^{r} + \lambda_i K_a\phi_{si}^{r} = 0 \\ K_s\phi_{si}^{r} + K_c\phi_{ai}^{r} + \lambda_i\left(\lambda_i M_s + C_s\right)\phi_{si}^{r} = 0 \\ K_a\phi_{ai}^{r} + \lambda_i^2 M_c\phi_{si}^{r} + \lambda_i^2 M_a\phi_{ai}^{r} = 0 \end{cases} \tag{48.28}$$

Since the first two equations in Eq. (48.28) are identically satisfied, Eq. (48.28) becomes

$$\begin{cases} K_s\phi_{si}^{r} + K_c\phi_{ai}^{r} + \lambda_i\left(\lambda_i M_s + C_s\right)\phi_{si}^{r} = 0 \\ K_a\phi_{ai}^{r} + \lambda_i^2 M_c\phi_{si}^{r} + \lambda_i^2 M_a\phi_{ai}^{r} = 0 \end{cases} \tag{48.29}$$

Comparing Eqs. (48.27) and (48.29), one has $a = \kappa$ and $b = -\frac{\kappa}{\lambda_i^2}$, where κ can be any non-zero constant. Hence, by Eq. (48.24), the left eigenvector η_i^l can be expressed by

$$\eta_i^l = \begin{Bmatrix} \phi_{si}^{l} \\ \phi_{ai}^{l} \\ \lambda_i\phi_{si}^{l} \\ \lambda_i\phi_{ai}^{l} \end{Bmatrix} = \kappa \begin{Bmatrix} \phi_{si}^{r} \\ -\frac{1}{\lambda_i^2}\phi_{ai}^{r} \\ \lambda_i\phi_{si}^{r} \\ -\frac{1}{\lambda_i}\phi_{ai}^{r} \end{Bmatrix} \tag{48.30}$$

For the convenience of discussion, let $\kappa = 1$, and one can obtain from Eq. (48.30) the relation between the structural components of the left and right eigenvectors:

$$\phi_{si}^{l} = \phi_{si}^{r} \tag{48.31}$$

and that between the acoustic components:

$$\phi_{ai}^{l} = -\frac{1}{\lambda_i^2}\phi_{ai}^{r} \tag{48.32}$$

48.2.2 FRFs

A sinusoidal force $Fe^{i\omega t}$ with frequency ω is applied on the structural part of the system described by Eq. (48.12), where $F = \left\{ F_s^T \; 0^T \right\}^T$ is an $(n+m)$-dimensional vector, in which $F_s = \left\{ f_{s1} \; f_{s2} \; \ldots \; f_{sn} \right\}^T$ is an n-dimensional structural force vector. Assuming a harmonic response of the system with frequency ω and canceling $e^{i\omega t}$ yield

$$(R + i\omega S)\,\eta = \left\{ \begin{array}{c} 0 \\ F \end{array} \right\} \tag{48.33}$$

A coordinate transformation is applied on η by letting

$$\eta = \Phi^r q \tag{48.34}$$

where $\Phi^r = \left[\eta_1^r \; \ldots \; \eta_{(m+n)}^r \; \eta_1^{r*} \; \ldots \; \eta_{(m+n)}^{r*} \right]$, in which the superscript $*$ denotes complex conjugation, is a matrix containing the right eigenvectors, and q is a $2\times(n+m)$-dimensional modal coordinate vector. Substituting Eq. (48.34) into Eq. (48.33), pre-multiplying the resulting expression by Φ^{lT}, where $\Phi^l = \left[\eta_1^l \; \ldots \; \eta_{(m+n)}^l \; \eta_1^{l*} \; \ldots \; \eta_{(m+n)}^{l*} \right]$ is a matrix containing the left eigenvectors, and applying the biorthonormality relations of the left and right eigenvectors in Eqs. (48.19)–(48.22) yield

$$\Lambda q = \Phi^{lT} \left\{ \begin{array}{c} 0 \\ F \end{array} \right\} \tag{48.35}$$

where $\Lambda = \mathrm{diag}\left[-\lambda_1 + i\omega, \ldots, -\lambda_{m+n} + i\omega, -\lambda_1^* + i\omega, \ldots, -\lambda_{m+n}^* + i\omega \right]$. The modal coordinate vector q can be obtained from Eq. (48.35):

$$q = \Lambda^{-1} \Phi^{lT} \left\{ \begin{array}{c} 0 \\ F \end{array} \right\} \tag{48.36}$$

Substituting Eq. (48.36) into Eq. (48.34) yields

$$\eta = \Phi^r q = \Phi^r \Lambda^{-1} \Phi^{lT} \left\{ \begin{array}{c} 0 \\ F \end{array} \right\} \tag{48.37}$$

The ratio of the pressure p_{ai} measured at point i in the acoustic field to the applied force f_{sj} at point j on the structure is

$$\frac{p_{ai}}{f_{sj}} = \sum_{h=1}^{m+n} \left(\frac{\lambda_h \phi_{ahi}^r \phi_{shj}^l}{-\lambda_h + i\omega} + \frac{\left(\lambda_h \phi_{ahi}^r \phi_{shj}^l \right)^*}{-\lambda_h^* + i\omega} \right) \tag{48.38}$$

Using Eq. (48.31) in Eq. (48.38) yields

$$\frac{p_{ai}}{f_{sj}} = \sum_{h=1}^{m+n} \left(\frac{\lambda_h \phi_{ahi}^r \phi_{shj}^r}{-\lambda_h + i\omega} + \frac{\left(\lambda_h \phi_{ahi}^r \phi_{shj}^r \right)^*}{-\lambda_h^* + i\omega} \right) \tag{48.39}$$

While the matrices $\tilde{M}$ and $\tilde{K}$ are non-symmetric, the modal characteristics of the system described by Eq. (48.3) are contained in Eqs. (48.38) and (48.39), and can be extracted from the FRFs in Eqs. (48.38) and (48.39) with the roving hammer technique using a well-developed modal analysis algorithm, such as PolyMax [18].

In the acoustic modal analysis in [6,7], it is assumed that the sound pressure linearly varies with the amplitude of vibration of the test structure at a certain frequency, which is proportional to the amplitude of excitation at an input point. Hence the sound pressure is proportional to the amplitude of excitation at the input point at a certain frequency, which can be validated by Eq. (48.38). It is further assumed in [6,7] that the amplitude of vibration of the test structure at a certain natural frequency varies with the modal coefficient of the input point, and the sound pressure per unit excitation force at the input point at the natural frequency is proportional to the modal coefficient of the input point. In Eq. (48.38), let $\omega = \omega_k$, where ω_k is

the natural frequency of the k-th mode of the structural-acoustic system; the sound pressure per unit excitation force at the natural frequency ω_k can be approximated by

$$\frac{p_{ai}}{f_{sj}} = \frac{\lambda_k \phi^l_{aki} \phi^l_{skj}}{-\lambda_k + i\,\omega_k} \tag{48.40}$$

where ϕ^l_{skj} is the modal coefficient of the input point j for the k-th mode, and the second assumption in the acoustic modal analysis in [6, 7] can be validated. Note that in the acoustic modal analysis in [6, 7], the measured natural frequencies of the test structure are the ones of the structural-acoustic system, and the measured mode shapes are the structural components of the left eigenvectors of the coupled system; this would also be the case for the VMT method, as illustrated below.

48.3 Modal Test Based on Vibro-Acoustic Reciprocity

Based on Eq. (48.38), the VMT method can measure the natural frequencies and the structural components of the left eigenvectors of the coupled system using an impact hammer and one or multiple sound pressure transducers. By Eqs. (48.31) and (48.39), the VMT method can measure the natural frequencies and the structural components of the right eigenvectors of the coupled system. Assuming that the natural frequencies and mode shapes of the structure in the structural-acoustic system described by Eq. (48.3) can be approximated by the natural frequencies and the structural components of the right eigenvectors of the coupled system, respectively, one can use the VMT method to measure the natural frequencies and mode shapes of the structure.

A vibro-acoustic reciprocity can be applied to a structural-acoustic system consisting of a linear elastic structure that is contiguous with air, based on which the transfer function between a structural force applied to the structure and the resulting sound pressure in rest contiguous air can be determined by exciting the structure with an omnidirectional point sound source and measuring the resulting acceleration of the structure [15]. The vibro-acoustic reciprocity is also referred to as Lyamshev reciprocity, and can be expressed by

$$\frac{p_{ai}}{f_{sj}} = -\frac{a_{sj}}{\dot{q}_{ai}} \tag{48.41}$$

where f_{sj} is the applied force to point j on the structure, p_{ai} is the measured sound pressure at point i in air induced by f_{sj}, $\dot{q}_{ai}$ is the volume acceleration of the point sound source at point i in air, and a_{sj} is the acceleration of point j on the structure induced by the point sound source. Note that f_{sj} and a_{sj} are in the same direction and $\dot{q}_{ai}$ represents the strength of the point sound source.

Based on the vibro-acoustic reciprocity, the VMT method is equivalent to the one where one or multiple omnidirectional point sound sources of known strengths are used to excite the structure and the resulting acceleration is measured. When the roving hammer technique is used, the measured mode shapes by the VMT method and EMA are in the directions of impacts. Since the impact directions are usually perpendicular to the surfaces being impacted, the merely in-plane modes cannot be excited by the VMT method and EMA, and only the out-of-plane components of mode shapes can be measured. A difference between the VMT method and EMA lies in the measurements of the dynamic responses of the structure since the former measures the pressure in air and the latter measures the acceleration of the structure. If one sound pressure transducer and one accelerometer are used in the VMT method and EMA, respectively, the FRFs from the former can be considered to be obtained by multiple inputs and a single output as if a point sound source and an accelerometer were used, according to Eq. (48.41), while those from the latter are obtained by a single input and a single output. Assuming that the excitation points are properly selected on the test structure and all the modes within a frequency range of interest can be excited, this difference enables the VMT method to capture all the out-of-plane modes of the structure of interest, including global and local ones, while EMA can miss some of the modes if the positions of the measurement points are improperly selected. The problem can occur when a measurement point in EMA is on a nodal line of a mode or in an inactive area of a local mode, which cannot be captured by the resulting FRFs. This problem will not occur in the VMT method, since the sound pressure transducer is located away from the test structure. Though the value of ϕ^r_{ahi} for a certain mode h in Eq. (48.39) can be relatively low, it does not vanish in that the pressure measured at the natural frequency ω_h by the sound pressure transducer does not vanish unless the excitation point is on a nodal line or in an inactive area of the mode. Use of multiple sound pressure sensors in the VMT method can help improve the measurement quality.

The VMT method is applicable to structures of any shapes when no noise is involved in the measurement of sound pressure. When noise is involved, the method may not be suitable for slender structures and structures with small surface areas. As illustrated in Fig. 48.1, the area of the surface of a structure facing an ideal point sound source is S_f; projecting

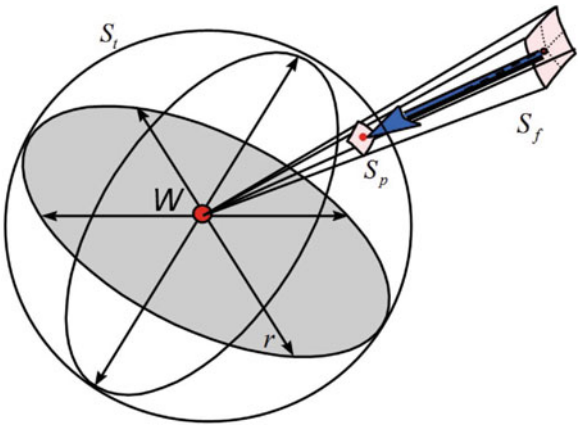

Fig. 48.1 Portion of the acoustic power from a point sound source with a power W transmitted to the area S_p projected from the surface of a structure facing the point source

the surface to a sphere with the center at the sound source, a constant radius r, and a surface area $S_t = 4\pi r^2$ gives a surface with an area S_p. The portion of the sound power that can reach the structure from the point source with a power W is βW, where $\beta = \frac{S_p}{S_t}$ is independent of r. A structure with a small value of β cannot be well excited by the point source, and the measured transfer functions between the strength of the point sound source and the resulting accelerations on the structure have low signal-to-noise ratios (SNRs). Consequently, based on the vibro-acoustic reciprocity, the measured FRFs in the VMT method using an ideal omnidirectional point sound pressure transducer at the location of the point sound source have low SNRs. Since the value of β is almost inversely proportional to the square of the distance between the sound pressure transducer and the structure, placing the sound pressure transducer close to the structure can increase the value of β. The sound pressure transducers should also be placed on the same side of the impacted surfaces of the structure to increase the SNRs of the measured FRFs. One should adjust the orientation of the structure so that a larger projected surface area can be obtained, which results in a larger β. However, for slender structures such as cables, and structures with small surface areas such as truss structures, the values of β can remain relatively small even if a sound pressure transducer is placed close to them. Hence the VMT method is more suitable for plate-like structures and structures with relatively large surface areas.

48.4 Experimental Validation

A case study was performed on an automotive disk brake using both the VMT method and EMA. The experimental results from the two methods were compared and validated using the FE model.

48.4.1 Test Setup

The disk brake was placed on foams, as shown in Fig. 48.2a, to simulate the free boundary conditions. For both the VMT method and EMA, the brake was excited at 146 points on the flange and in the bolted area, as shown in Fig. 48.2b, using a PCB 086D80 impact hammer. The excitation direction was perpendicular to the brake surfaces. In order to distinguish some of the modes with close natural frequencies due to almost axial-symmetry of the brake, multiple random impacts [16] were given at every excitation point for 4 s in each test, which results in a frequency resolution of 0.25 Hz, and three tests were averaged to ensure repeatable results with a good coherence. The responses of the brake were measured using one PCB U130D20 and two PCB 130E20 microphones and four PCB 352C66 accelerometers for the VMT method and EMA, respectively; the data were collected using a 36-channel LMS spectrum analyzer. For the VMT method, the three microphones were placed at fixed locations near the brake and pointing towards it, as shown in Fig. 48.2a. For EMA, two sets of tests were conducted; the four accelerometers were attached in one set of tests on the bottom surface of the flange, and in the other set of tests on the bottom surface of the bolted area. Note that the microphones used in the VMT method here are of the free-field type, whose measurements are most accurate when the sound pressure from a single source and a single direction is measured [17]. Since the flange and the bolted area of the brake are flat surfaces, and the microphones were placed not too close to the brake and pointing towards the brake, the measurements of the sound pressure by the microphones can be used in the VMT method by assuming that the sound pressure in the directions perpendicular to those in which the microphones can accurately measure the sound pressure can be neglected.

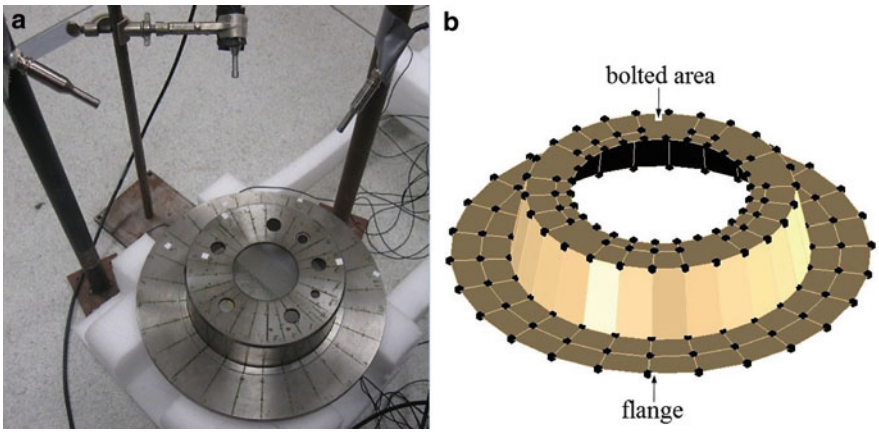

Fig. 48.2 (**a**) Test setup for the VMT method, and (**b**) excitation points for the VMT method and EMA

Table 48.1 Measured natural frequencies of the disk brake by the VMT method and EMA

Mode	VMT frequency (Hz)	EMA frequency (Hz)	Frequency difference (%)
1	1,072.4	1,064.5	0.74
2	1,073.8	1,070.2	0.34
3	1,237.2	1,231.0	0.50
4	1,576.5	1,574.5	0.13
5	1,576.7	1,578.1	−0.09
6	1,617.4	1,608.9	0.53
7	1,620.4	1,612.8	0.47
8	2,004.4	2,003.2	0.06
9	2,115.5	2,113.3	0.10
10	2,115.9	2,114.1	0.09
11	2,428.3	2,412.1	0.67
12	2,429.3	2,421.0	0.34
13	2,591.6	2,591.0	0.02
14	2,600.8	2,600.2	0.02
15	3,504.0	3,503.3	0.02
16	3,504.1	3,503.4	0.02
17	3,918.8	3,918.1	0.02
18	3,940.5	3,938.7	0.05

48.4.2 Results and Discussion

Modal analysis was conducted using PolyMax [18] in the LMS Test.Lab Rev. 9b; the measured natural frequencies and mode shapes of the brake by the VMT method were extracted from three sets of measured FRFs from the three microphones, and those by EMA from eight sets of measured FRFs from the four accelerometers. The highest natural frequency of the rigid body modes of the brake in the tests is 36.75 Hz, which is lower than 10% of the natural frequency of the first elastic mode, and the boundary conditions can be considered to be free [1]. In order to experimentally validate the assumption in Sect. 48.3 that the natural frequencies and mode shapes of the structure can be approximated by the natural frequencies and the structural components of the right eigenvectors of the coupled system, respectively, the natural frequencies of the first 18 elastic modes of the brake from the VMT method and EMA were compared in Tables 48.1 and 48.2, respectively, and the maximum natural frequency difference is 0.74%. The differences between the two sets of measured natural frequencies mainly derive from mass loading introduced by the accelerometers in EMA, since all of the measured natural frequencies from EMA, except that of the fifth elastic mode, are lower than the corresponding ones from the VMT method; the measured natural frequency of the fifth elastic mode from EMA is higher than that from the VMT method due to measurement error. The MAC values of the associated mode shapes, which are the diagonal entries of the MAC matrix [1] in Table 48.2, are all over 90%. Some off-diagonal entries in Table 48.2 are relatively high due to two reasons. One reason is that the number of excitation points is not large enough and some mode shapes cannot be well distinguished from others. The second reason is that the mode shapes were not measured in three dimensions in the tests using the two methods. The impact hammer excited the brake in the direction perpendicular to the surfaces of the flange and the bolted area, and only the out-of-plane mode

Table 48.2 Entries of the MAC matrix in percent corresponding to the first 18 measured mode shapes of the disk brake by the VMT method and EMA; the horizontal and vertical mode numbers correspond to the measured modes by the VMT method and EMA, respectively

Mode	1	2	3	4	5	6	7	8	9	10	11	12	13	14	15	16	17	18
1	96	49	6	4	4	6	2	1	17	29	11	2	0	0	4	2	1	2
2	41	95	5	2	7	7	4	1	32	28	5	3	0	1	2	3	4	3
3	10	3	98	17	7	5	0	57	5	5	4	3	5	8	1	5	3	8
4	1	2	8	92	34	2	8	9	3	6	1	3	45	22	2	5	3	3
5	0	8	4	29	91	13	13	3	4	2	3	0	18	21	1	3	0	2
6	3	4	2	10	3	91	28	1	2	3	5	10	3	2	2	2	1	1
7	2	7	2	3	9	46	97	1	2	3	3	6	2	3	5	3	1	1
8	1	1	64	9	5	2	1	100	7	3	3	2	7	7	1	1	5	11
9	20	25	6	3	11	4	5	8	90	16	5	4	1	1	4	2	25	2
10	26	37	6	2	2	7	2	4	40	94	4	2	2	3	1	1	15	25
11	9	6	4	2	4	7	2	1	5	6	92	29	3	3	8	7	1	1
12	3	6	3	3	2	6	4	0	2	7	43	96	0	0	6	12	0	1
13	0	0	3	36	20	0	1	2	0	2	5	3	91	11	1	1	5	3
14	0	0	7	17	36	3	5	6	1	3	2	0	28	99	1	1	7	5
15	1	3	3	3	1	3	5	0	1	3	2	5	0	0	95	14	0	1
16	3	2	0	1	2	6	3	0	2	4	6	6	0	0	26	94	1	0
17	1	2	5	4	2	0	0	8	31	9	1	1	11	8	2	2	94	11
18	3	1	7	2	4	0	1	7	9	34	1	0	13	4	0	0	34	97

shapes were measured; one cannot excite the brake in the directions parallel to the surfaces of the flange and the bolted area and the interior points of the brake. If the in-plane components of two distinct modes are not measured, their out-of-plane components can be similar and the corresponding MAC value of the two mode shapes can be relatively high [19].

The sums of the measured FRFs in the neighborhoods of the first two elastic modes by the VMT method and EMA are shown in Fig. 48.3a, where the measurements are from a microphone away from the brake and an accelerometer on the flange, respectively. Since the brake is almost axial-symmetric, there are pairs of close frequencies, and the associated peaks in the measured FRFs can be close to each other or overlapped depending on the frequency resolution used. As shown in Fig. 48.3a, there is only one peak that can be observed in the summed FRF from the VMT method, from which two distinct modes can be identified by the modal analysis software and their natural frequency difference is 1.6 Hz. The actual natural frequency difference between the two modes may be smaller than 1.6 Hz and two separate peaks representing the two close natural frequencies may be observed if a higher frequency resolution is used in the test. On the other hand, there are two separate peaks corresponding to the two modes in the summed FRF from EMA due to mass loading from the accelerometers, which increases the natural frequency difference to 5.7 Hz. Hence the VMT method is more suitable for an axial-symmetric structure since it can preserve close natural frequencies of the structure due to axial-symmetry.

The sums of the measured FRFs by EMA, where the measurement points are on the flange and in the bolted area of the brake, and that of the measured FRFs by the VMT method are shown in Fig. 48.3b. As shown in Fig. 48.3b, the peaks corresponding to modes 11 and 12 cannot be identified in the summed FRF for which the measurement point is in the bolted area; the same observation can be made for modes 15 and 16. The reason is that the bolted area is inactive for the four modes, whose vibrations cannot be measured by the accelerometer. On the other hand, the peaks corresponding to the four modes can be clearly identified in the summed FRF by the VMT method. The peaks corresponding to modes 17 and 18 cannot be observed in the two summed FRFs for which the measurement points were on the flange and in the bolted area, respectively. However, the peaks corresponding to the two modes can be clearly identified in the summed FRF from the VMT method, as shown in Fig. 48.3b, since the VMT method can capture all the out-of-plane modes, including global and local ones. In the VMT method, the pressure measured by a microphone is from the vibration of the impacted surface of the brake; the quality of the pressure measurement would not be affected much by the nodal lines and local modes of the brake. If the locations of the microphones and the orientation of the brake relative to the microphones comply with the guidelines in Sect. 48.3, the VMT method would be more efficient than EMA.

In order to validate the experimental results, an intensive FE model of the brake was created using solid tetrahedral elements in the commercial FE software Abaqus 6.9 EF. The brake is made of cast iron Class 25 with an elastic modulus of 113.7 GPa, a Poisson's ratio of 0.28, and a mass density of 7,200 kg/m^3. The profile and the FE model of the brake are shown in Fig. 48.4. Note that the unit in the profile is mm.

The calculated natural frequencies of the first 18 elastic modes of the brake from the FE model and the measured ones by the VMT method and EMA are shown in Table 48.3. The errors between the measured natural frequencies by the VMT method and EMA and the calculated ones from the FE model are less than 3%, except that the error for the 11th elastic mode

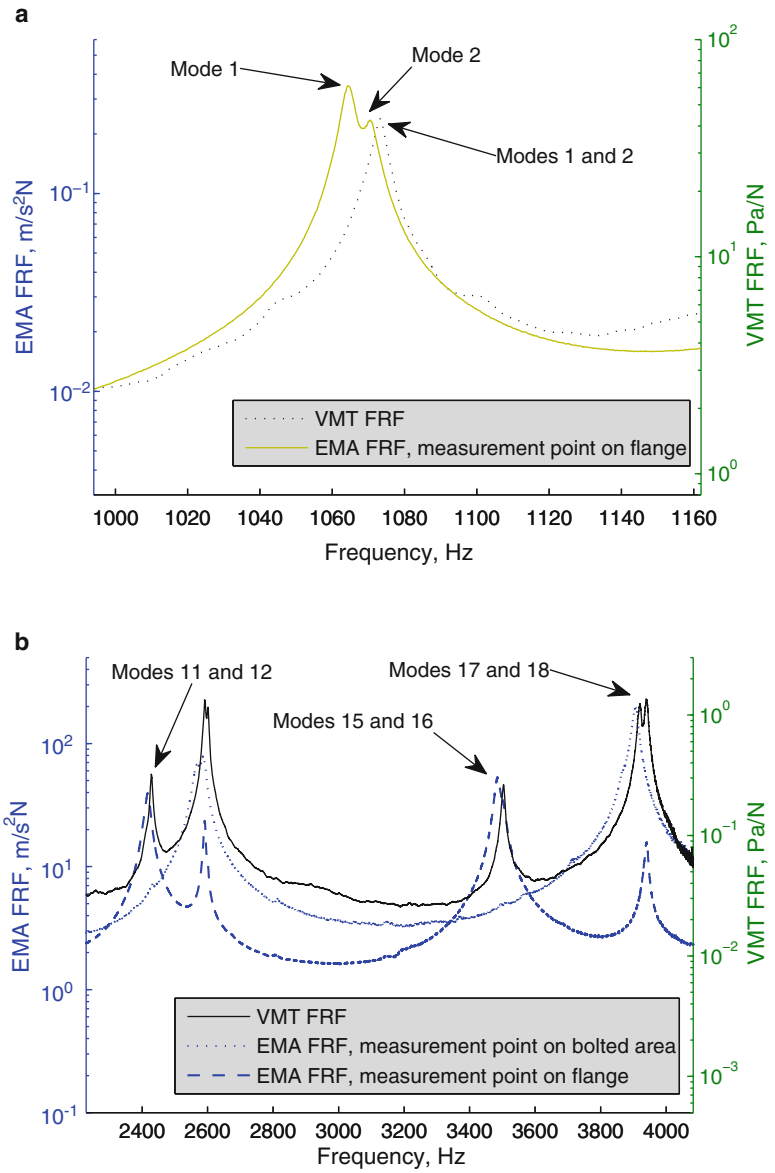

Fig. 48.3 (**a**) Summed FRFs by the VMT method and EMA in the neighborhood of the first two elastic modes, and (**b**) summed FRFs by the VMT method and EMA from 2,250 Hz to 4,050 Hz

by EMA is 3.26%. The calculated three-dimensional mode shapes from the FE model and the measured out-of-plane ones by the VMT method are shown in Table 48.4. Note that the in-plane components of the calculated eighth and ninth elastic mode shapes in Table 48.4 are relatively large compared to their out-of-plane ones. Note also that the eighth through tenth modes from the VMT method and EMA in Table 48.1 correspond to the tenth, eighth, and ninth modes from the FE model, respectively, and the order for the three modes from the VMT method and EMA has been shifted in Tables 48.3 and 48.4 according to that of the FE model. The MAC matrices for the out-of-plane components of the measured mode shapes by the VMT method and EMA and the calculated ones from the FE model are shown in Tables 48.5 and 48.6, respectively; the MAC values of the associated mode shapes are all over 90%.

48.5 Conclusion

The VMT method developed here is based on the assumption that the natural frequencies and mode shapes of the test structure can be approximated by the natural frequencies and the structural components of the right eigenvectors of the structurally damped structural-acoustic system, respectively. The coupling between the structure and the acoustic field in a structural-acoustic system introduces asymmetry in the model formulation. The associated eigenvalue problem is derived

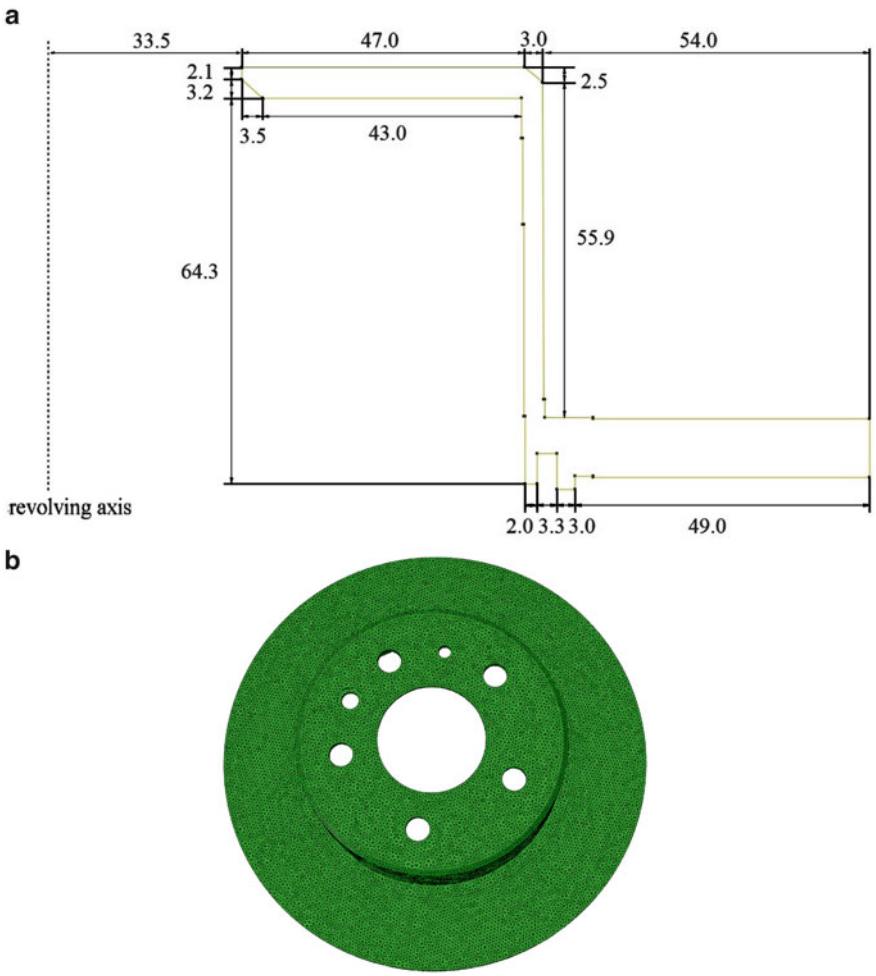

Fig. 48.4 (**a**) The profile and (**b**) the FE model of the disk brake

Table 48.3 Comparison of measured natural frequencies by the VMT method and EMA with the calculated ones from the FE model

Mode	Numerical frequency (Hz)	VMT frequency (Hz)	Error (%)	EMA frequency (Hz)	Error (%)
1	1,062.5	1,072.4	0.93	1,064.5	0.19
2	1,062.7	1,073.8	1.04	1,070.2	0.71
3	1,236.7	1,237.2	0.03	1,231.0	−0.46
4	1,593.3	1,576.5	−1.05	1,574.5	−1.18
5	1,594.0	1,576.7	−1.09	1,578.1	−1.00
6	1,651.1	1,617.4	−2.04	1,608.9	−2.56
7	1,651.3	1,620.4	−1.87	1,612.8	−2.33
8	2,055.3	2,115.5	2.93	2,113.3	2.82
9	2,055.5	2,115.9	2.94	2,114.1	2.85
10	2,061.8	2,004.4	−2.78	2,003.2	−2.84
11	2,493.3	2,428.3	−2.61	2,412.1	−3.26
12	2,493.6	2,429.3	−2.58	2,421.0	−2.91
13	2,656.5	2,591.6	−2.44	2,591.0	−2.47
14	2,666.7	2,600.8	−2.47	2,600.2	−2.49
15	3,601.3	3,504.0	−2.70	3,503.3	−2.72
16	3,601.5	3,504.1	−2.70	3,503.4	−2.72
17	3,995.1	3,918.8	−1.91	3,918.1	−1.93
18	4,015.1	3,940.5	−1.86	3,938.7	−1.90

Table 48.4 Mode shapes of the first 18 elastic modes of the brake from the FE model and the VMT method

Mode	FE Mode Shape	VMT Mode Shape	Mode	FE Mode Shape	VMT Mode Shape
1	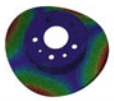		10	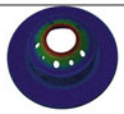	
2	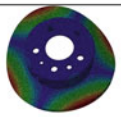		11	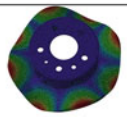	
3	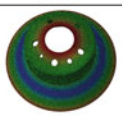		12	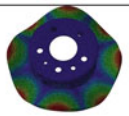	
4	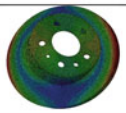		13	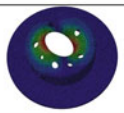	
5	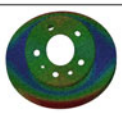		14	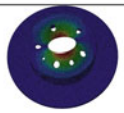	
6	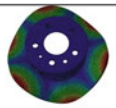		15	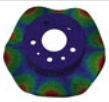	
7	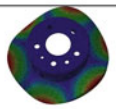		16	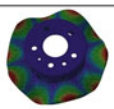	
8	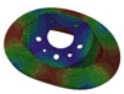		17	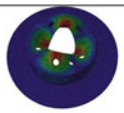	
9	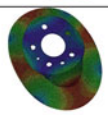		18	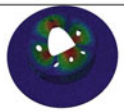	

using an equivalent state space formulation for the coupled system. The biorthonormality relations between the left and right eigenvectors and the relations between the structural and acoustic components in the left and right eigenvectors are proved. The FRFs used in the VMT method are derived, which contain the modal characteristics of the coupled system. Based on the vibro-acoustic reciprocity, the VMT method can measure all the out-of-plane modes and its measurement quality would not be affected by a nodal line of a mode and an inactive area of a local mode of the structure; the guidelines for using the VMT method, including the types of structures that are suitable for the method, the positions of the sound pressure transducers, and the orientation of the test structure relative to the transducers, are provided. Modal tests were carried out on an automotive disk brake using the VMT method and EMA, where multiple microphones and accelerometers were used to measure its dynamic responses induced by impacts, respectively. The differences between the measured natural frequencies of the first 18 elastic modes by the VMT method and EMA are less than 1% and the MAC values of the associated mode shapes are all above 90%. The errors between the measured natural frequencies by the VMT method and those from the FE model are less than 3% for the first 18 elastic modes, and the MAC values of the associated mode shapes are all above 90%. It is shown that the VMT method can not only preserve close natural frequencies of the brake due to axial-symmetry, but also measure all the out-of-plane modes within the frequency range of interest, including global and local ones.

Table 48.5 Entries of the MAC matrix in percent corresponding to the first 18 calculated mode shapes of the disk brake from the FE model and the measured ones by the VMT method; the horizontal and vertical mode numbers correspond to the calculated and measured modes, respectively

Mode	1	2	3	4	5	6	7	8	9	10	11	12	13	14	15	16	17	18
1	96	15	5	1	3	11	2	2	23	49	6	7	0	0	6	6	1	2
2	29	91	3	4	5	17	8	1	36	45	4	9	0	0	2	4	1	1
3	2	3	99	1	3	1	1	54	4	1	0	5	5	4	1	6	5	6
4	10	2	16	90	32	3	7	7	6	6	7	8	39	4	5	9	2	3
5	8	5	7	9	93	9	11	5	4	7	3	1	5	37	0	3	4	4
6	8	1	3	2	8	92	22	2	1	6	16	3	1	3	6	7	0	0
7	5	6	2	11	13	16	94	1	4	1	3	15	1	4	3	8	0	1
8	0	1	70	3	2	0	0	99	1	0	0	1	5	2	0	1	7	7
9	19	33	7	4	2	6	4	7	91	24	4	1	1	0	2	4	35	11
10	28	20	4	6	2	9	3	3	26	90	5	8	2	3	1	1	20	34
11	1	6	4	2	3	6	1	2	4	2	94	16	6	3	12	18	1	1
12	5	2	2	1	2	8	7	2	2	2	28	92	3	1	11	12	1	0
13	1	0	6	43	19	1	1	7	2	3	1	1	98	13	0	0	5	12
14	0	0	7	28	33	1	0	8	1	3	0	1	33	91	0	0	9	8
15	5	2	1	2	1	4	5	1	2	2	3	10	1	1	94	15	2	1
16	3	3	5	5	3	4	4	2	3	2	10	15	2	1	8	90	1	1
17	1	3	2	3	2	1	0	4	27	6	1	0	6	5	0	1	97	9
18	3	2	9	4	1	0	0	11	6	26	1	1	7	4	1	0	34	93

Table 48.6 Entries of the MAC matrix in percent corresponding to the first 18 calculated mode shapes of the disk brake from the FE model and the measured ones by EMA; the horizontal and vertical mode numbers correspond to the calculated and measured modes, respectively

Mode	1	2	3	4	5	6	7	8	9	10	11	12	13	14	15	16	17	18
1	95	18	5	2	3	12	4	2	19	51	10	6	0	0	3	3	0	1
2	25	95	3	1	2	12	3	1	41	41	9	6	0	0	1	6	2	1
3	4	3	98	0	4	2	1	48	1	4	3	4	3	5	1	7	5	6
4	2	2	7	90	36	2	2	8	1	4	5	4	41	6	3	5	2	4
5	7	1	3	19	96	11	3	5	3	4	3	1	18	27	2	4	0	1
6	5	10	3	5	7	95	14	1	7	2	8	6	3	4	4	3	1	0
7	4	8	0	8	8	28	93	1	6	1	3	12	1	3	2	4	1	0
8	1	0	71	2	2	0	0	99	1	0	0	1	3	3	0	1	7	7
9	23	38	6	2	9	4	2	7	94	14	6	1	0	0	2	4	31	10
10	24	27	7	3	2	7	4	3	31	90	5	5	1	3	1	3	17	29
11	11	2	3	1	4	7	2	1	3	8	93	8	2	3	12	14	0	1
12	3	1	2	1	1	2	7	1	2	1	29	92	0	0	16	11	0	0
13	0	0	3	34	33	0	0	4	1	1	1	1	91	46	0	0	2	4
14	0	0	6	26	35	0	0	7	1	3	1	0	26	94	0	0	10	7
15	5	1	2	2	2	7	3	1	1	2	8	10	0	0	94	2	0	0
16	1	1	0	1	3	2	3	0	0	2	8	7	0	0	24	90	0	0
17	1	2	6	4	1	0	0	8	29	2	0	0	9	2	0	0	95	18
18	1	2	7	5	1	0	0	8	5	30	0	0	10	1	0	0	33	95

References

1. Ewins DJ (2001) Modal testing: theory, practice and application, 2nd edn. Wiley, England
2. Van der Auweraer H (2001) Structural dynamics modeling using modal analysis: applications, trends and challenges. In: IEEE instrumentation and measurement technology conference, Budapest, 21–23 May 2001
3. Yang QJ, Lim GH, Lin RM, Yap FF, Pang HLJ, Wang ZP (1997) Experimental modal analysis of PBGA circuit board assemblies. In: IEEE/CPMT electronic packaging technology conference, Singapore
4. Ashory MR (2002) Assessment of the mass-loading effects of accelerometers in modal testing. In: Proceedings of the IMAC XX, Los Angeles, CA
5. Vanlanduit S, Daerden F, Guillaume P (2007) Experimental modal testing using pressurized air excitation. J Sound Vib 299:83–98
6. Allemang R, Shapton W (1978) Using modal techniques to guide acoustic signature analysis. SAE Technical Paper 780106
7. Elwali W, Satakopan H, Shauche V, Allemang R, Phillips A (2010) Modal parameter estimation using acoustic modal analysis. In: Proceedings of the IMAC XXVIII, Jacksonville, FL
8. Craggs A (1969) The transient response of coupled acousto-mechanical systems. NASA Contractor Report: CR 1421

9. Luo J, Gea HC (1997) Modal sensitivity analysis of coupled acoustic-structural systems. J Vib Acoust 119:545–550
10. Ma ZD, Hagiwara I (1991) Sensitivity analysis methods for coupled acoustic-structural systems part I: modal sensitivities. AIAA J 29(11):1787–1795
11. Wyckaert K, Augusztinovicz F, Sas P (1996) Vibro-acoustical modal analysis: reciprocity, model symmetry, and model validity. J Acoust Soc Am 100(5):3172–3181
12. Xing J-T, Price WG (1991) A mixed finite element method for the dynamic analysis of coupled fluid-solid interaction problems. Proc R Soc 433(1888):235–255
13. Sung SH, Nefske DJ, Feldmaier DA (2009) A structural-acoustic finite element method for predicting automotive vehicle interior road noise. In: Proceedings of the ASME 2009 international mechanical engineering congress & exposition, Lake Buena Vista, 13–19 November 2009
14. Meirovitch L (1997) Principles and techniques of vibrations. Prentice Hall, Upper Saddle River
15. Fahy FJ (2003) Some applications of the reciprocity principle in experimental vibroacoustics. Acoust Phys 49(2):217–229
16. Zhu WD, Zheng NA, Wong CN (2007) A Stochastic model for the random impact series method in modal testing. ASME J Vib Acoust 129:265–275
17. PCB Piezotronics Inc., Microphone handbook: test and measurement microphones. PCB Piezotronics, Depew
18. Guillaume P, Verboven P, Vanlanduit S, Van der Auweraer H, Peeters B (2003) A poly-reference implementation of the least-squares complex frequency-domain estimator. Proceedings of the IMAC XXI, Kissimmee, FL
19. Heylen W, Lammens S, Sas P (1998) Modal analysis theory and testing. Katholieke Universiteit Leuven, Belgium